# An *in situ* method for diagnosing phase shifting interferometry



2016 JINST 11 P05018

(http://iopscience.iop.org/1748-0221/11/05/P05018)

Published by IOP Publishing for Sissa Medialab

Received: *February 26, 2016*
Accepted: *May 2, 2016*
Published: *May 24, 2016*



# An *in situ* method for diagnosing phase shifting interferometry

**J. Shao,**[a,b,1] **D. Ma,**[b] **H. Zhang**[b] **and Y. Xie**[b]

[a] *College of Mechanical Engineering, Qingdao Technological University, Jia Lingjiang Road No. 777, Qingdao, China*

[b] *State Key Laboratory of Applied Optics, Changchun Institute of Optics, Fine Mechanics and Physics, Chinese Academy of Sciences, Dong Nanhu Road No. 3888, Changchun, China*

*E-mail:* qunying12@163.com

Abstract: Current diagnosing phase shifting interferometry is a time and funds consuming process. Hence a brief and effective method is necessary to satisfy the real-time testing. In this paper, mathematical solutions for errors were deduced from the difference of intensity patterns. Based on the diversity of error distributions, an effective method for distinguishing and diagnosing the error sources is proposed and verified by an elaborative designed simulation. In the actual comparison experiment, vibration, phase-shift error and intensity fluctuation were imposed to demonstrate this method. The results showed that this method can be applied into the real-time measurement and provide an *in situ* diagnosing technique.

Keywords: Interferometry; Optics; Real-time monitoring

[1] Corresponding author.



doi:10.1088/1748-0221/11/05/P05018

## Contents



2016 JINST 11 P05018

## 1 Introduction

The phase shifting interferometer is a widely used optical testing instrument with high accuracy [1, 2]. Its systematic errors in the reference can be calculated by absolute testing, achieving an accuracy of 0.1 nm [3]. However, its precision always suffers from various error sources, whose effect can be reduced by average methods [4] but cannot be eliminated. When the precision exceeds strict limits, the worn components should be repaired or replaced. The remaining problems are to determine what are influencing the precision and where the error sources lie. Generally, this process is costly and time-consuming. A brief and effective *in situ* method is necessary.

To diagnose error sources, the characteristics of different errors must be analyzed. During the past decades, various algorithms have been used to investigate the errors in phase shifting interferometry [5–7]. J. Schwider developed error source formulas for phase-shift error and vibration, based on a common 5-step algorithm [5]. J. van Wingerden gave the formulas of the errors in a linear approximation considering light source instability, imperfect phase shifting, mechanical vibrations, nonlinearity of the detector, and quantization of the detector signal [7]. Meanwhile, H. Schreiber and J.H. Bruning summarized the error functions [8]. However, these solutions are based on 3~5 step algorithms. Fourier description of digital phase shifting interferometry was applied [9, 10]. Based on Fourier analysis, C.P. Brophy studied the phase error caused by intensity instability [11]. But this solution is complicated and does not fit to the description of other errors. Peter J. de Groot focused on the amount of errors and proposed the phase-error transfer function caused by vibration [12]. The 2D error distribution is more intuitive for error diagnosing. A simple and universal solution is needed.

First, variations of intensity patterns caused by different error sources were assorted in section 2. Built on the diversity of intensity patterns, the error distributions are distinct and can be

distinguished. In section 3, the mathematical solutions of errors were derived. To demonstrate these solutions, the various error distributions were simulated and shown in section 4. The simulation proves that different error sources will cause the diversity of error distributions. An *in situ* method for diagnosing the error sources is proposed. To verify this method, a comparison experiment was implemented. In section 5, the vibration, phase-shift error and intensity fluctuation were imposed separately, and the diversity of error distributions was distinguished.

## 2 Error sources in phase shifting interferometry

In a phase shifting interferometer, the sample beam and reference beam combine together. The path difference, i.e., the difference in the distance traveled by each beam, creates a phase difference between them, which in turn creates an interference pattern. If the optical path is changed artificially (phase shifting), the phase can be reconstructed from a set of interference patterns based on a phase shifting algorithm.

For two-beam interferometry with the same frequency, the pattern of interference fringes $I_n$ can be written as follows:

$$I_n(\varphi, t) = 1 + V \times \cos(\varphi + \phi_n). \tag{2.1}$$

$V$ is the contrast of the interference fringes, $\phi_n$=$2\pi v_0 t$ is the phase shifting at the time $t$, $v_0$ is the frequency, $n$ is the frame sequence, and $\varphi$ is the tested phase difference between the two beams. Phase shifting algorithms extract the phase from the intensity patterns. The phase extraction function is

$$\varphi = \tan^{-1} \frac{\sum\limits_n I_n s_n}{\sum\limits_n I_n c_n}, \tag{2.2}$$

where $s_n$ and $c_n$ are the weight factors of the filter function. Literature [13] show a relationship between $s_n$ and $c_n$:

$$\begin{aligned} s_n &= w_n \sin(-\phi_n), & c_n &= w_n \cos(\phi_n); \\ \sum_n s_n &= 0, & \sum_n c_n &= 0; \\ \sum_n s_n \sin(-\phi_n) &= \sum_n c_n \cos(\phi_n); \\ \sum_n s_n \cos(\phi_n) &= -\sum_n c_n \sin(-\phi_n), \end{aligned} \tag{2.3}$$

where $w_n$ is the real window function. Eq. (2.2) can be derived to different phase shifting algorithms.

But there are many error sources reduce the measurement accuracy, such as manufacture error in the reference surface, phase-shift error caused by the piezoelectric transducer, position deviation caused by vibration, unstable intensity of the light source (laser), and frequency fluctuation of the light source. These error sources vary the intensity patterns, and the result of phase extraction will be changed. Meanwhile, the manufacture error in the reference is a systematic error, which can be eliminated by absolute calibration. However, Phase-shift error, position deviation caused by vibration, unstable intensity of laser and frequency fluctuation of laser are unusual error sources.



2016 JINST 11 P05018

Their error will vary on the tested phase $\varphi$ so that they are difficult to deal with. These error sources are what we focus on.

First, the variation of intensity patterns caused by error sources should be studied. If these error sources are considered, the interference pattern in eq. (2.1) will become

$$I'_n(\varphi, t) = I_n(\varphi, t) + \Delta I_n(\varphi, t). \tag{2.4}$$

a) For the case of phase-shift error caused by the error in the piezoelectric transducer or piston vibration along the Z axis, the intensity is

$$I'_n(\varphi, t) = 1 + V \times \cos(\varphi + \phi_n + \Delta P_n)\,. \tag{2.5}$$

$\Delta P_n$ is the phase-shift error at step $n$, and $\phi_n$ is the phase at the step $n$.

b) For the case of position deviation caused by tip-tilt vibration in the $(x, y)$ plane,

$$\begin{aligned} I'_n(\varphi, t) &= 1 + V \times \cos(\varphi(x + \Delta x, y + \Delta y) + \phi_n) \\ &\approx 1 + V \times \cos\left(\varphi(x, y) + \frac{\mathrm{d}^2\varphi(x, y)}{\mathrm{d}x\mathrm{d}y}\Delta x \Delta y + \phi_n\right)\,. \end{aligned} \tag{2.6}$$

$\Delta x$, $\Delta y$ are the displacement.

c) For the case of unstable intensity of the light source,

$$I'_n(\varphi, t) = (1 + \Delta_n I) \times (1 + V \times \cos(\varphi + \phi_n)), \tag{2.7}$$

$\Delta_n I$ is the intensity instability at step $n$.

d) For the case of frequency fluctuation of the light source,

$$I'_n(\varphi, t) = 1 + V \times \cos\left((1 + \Delta_n f) \times (\varphi + \phi_n)\right). \tag{2.8}$$

$\Delta_n f$ is the frequency variation of the light source.

Based on eqs. (2.6)–(2.8), it is obvious that various error sources have different intensity patterns, and it is believed that different error sources cause the diversity of error distributions.

## 3 Relationship between errors and error sources

The error will change as the variations of intensity patterns caused by different error sources. $\Delta I_n$ is the variation of the intensity patterns caused by different error sources and it can be evaluated by

$$\Delta I_n = I'_n - I_n \approx \left(\mathrm{d}I_n \Big/ \mathrm{d}x\right)\mathrm{d}x, \tag{3.1}$$

where $x$ is the variable parameter caused by error source. The extracted phase $\varphi$ changed into the following equation:

$$\tan\varphi' = \frac{\sum\limits_n (I_n + \Delta I_n)\, s_n}{\sum\limits_n (I_n + \Delta I_n)\, c_n} = \frac{N'}{D'}, \qquad \varphi' = \tan^{-1}\frac{N'}{D'}, \tag{3.2}$$



2016 JINST 11 P05018

where $N' = \sum (I_n + \Delta I_n)\, s_n$, $D' = \sum (I_n + \Delta I_n)\, c_n$. Using the formulas $\mathrm{d}\left[\tan^{-1}(\delta)\right] \Big/ \mathrm{d}\delta = 1\Big/\left(1+\delta^2\right)$, $\delta = \tan\varphi$ and $\sin 2\varphi = 2\tan\varphi\Big/\left(1+\tan^2\varphi\right)$, the measurement error is calculated as follows:

$$\begin{aligned}
\Delta\varphi = \varphi' - \varphi \approx \frac{\mathrm{d}\tan^{-1}(\delta)}{\mathrm{d}\delta}\Delta\delta &= \frac{\sin 2\varphi}{2\tan\varphi} \times [\tan(\varphi') - \tan(\varphi)] \\
&= \frac{\sin 2\varphi}{2\tan\varphi} \times \left(\frac{N'}{D'} - \tan\varphi\right) \\
&= \frac{\sin 2\varphi}{2}\left(\frac{N'}{\tan\varphi \times D'} - 1\right) \\
&= \frac{\sin 2\varphi}{2}\left\{\frac{\sum\limits_{n1}(I_{n1} + \Delta I_{n1})\, s_{n1} \times \sum\limits_{n2} I_{n2}c_{n2}}{\sum\limits_{n1}(I_{n1} + \Delta I_{n1})\, c_{n1} \times \sum\limits_{n} I_{n2}s_{n2}} - 1\right\} \\
&\approx \frac{\sin 2\varphi}{2}\frac{\sum\limits_{n}\Delta I_n s_n \times \sum\limits_{n} I_n c_n - \sum\limits_{n}\Delta I_n c_n \times \sum\limits_{n} I_n s_n}{\left(\sum\limits_{n} I_n s_n\right)\left(\sum\limits_{n} I_n c_n\right)} \\
&= k\left[\sum_n \Delta I_n s_n \times \cos\varphi - \sum_n \Delta I_n c_n \times \sin\varphi\right].
\end{aligned} \tag{3.3}$$

Here is an approximation that makes this solution brief and efficient.

In eq. (3.3), $k$ is a constant, and we set $k$= 1 to analyze the 2D error distribution $\Delta\varphi$. The errors in the phase shifting interferometer are discussed below based on eqs. (3.1) and (3.3).

For the case of phase-shift error caused by the detuning error of the piezoelectric transducer or introduced by the vibration along the $z$ axis (ray axis), the variation of the intensity patterns $\Delta I_n$ is

$$\Delta I_n(\varphi) = I'_n - I_n \approx -V \times \sin(\varphi + \phi_n) \times \Delta P_n. \tag{3.4}$$

$\Delta P_n$ is the phase-shift error at step $n$, and $\phi_n$ is the phase at the step $n$. The phase error $\Delta\varphi$ is

$$\Delta\varphi = \sum_n \Delta P_n \times V\frac{w_n}{2}\left[1 - \cos\left(2\varphi + 2\phi_n\right)\right]. \tag{3.5}$$

This solution coincides with the eq. (45) of literature [9], if the approximation is neglected.

For the case of position deviation caused by vibration in the $(x, y)$ Cartesian coordinates plane, the variation of the intensity patterns $\Delta I_n$ is

$$\Delta I_n(x, y) = I'_n - I_n \approx -V \times \sin(\varphi + \phi_n) \times \frac{\mathrm{d}^2\varphi}{\mathrm{d}x\mathrm{d}y}\Delta x\Delta y, \tag{3.6}$$

where $\Delta x$, $\Delta y$ are the displacement. The phase error $\Delta\varphi$ is

$$\Delta\varphi = \sum_n \frac{\mathrm{d}^2\varphi}{\mathrm{d}x\mathrm{d}y}\Delta x\Delta y V\frac{w_n}{2}\left[1 - \cos\left(2\varphi + 2\phi_n\right)\right]. \tag{3.7}$$

For the case of unstable intensity of the light source, the variation of the interference patterns $\Delta I_n$ is

$$\Delta I_n(\varphi) = \Delta_n I \times (1 + V \times \cos(\varphi + \phi_n)), \tag{3.8}$$



2016 JINST 11 P05018

where $\Delta_n I$ is the intensity instability at step $n$. Replace $\Delta I_n$ in eq. (2.8) with eq. (3.8), and the error $\Delta\varphi$ is formulated as

$$\Delta\varphi = \sum_n \Delta_n I\,(-w_n)\left[\sin(\varphi+\phi_n) + \frac{V}{2}\sin(2\varphi+2\phi_n)\right]. \tag{3.9}$$

This solution coincides with the eq. (2.7) of literature [11], if the approximation is neglected.

For the case of frequency fluctuation of the light source, the variation of the intensity patterns $\Delta I_n$ is

$$\Delta I_n(\varphi) = -V\sin(\varphi+\phi_n)\times(\varphi+\phi_n)\times\Delta_n f\,. \tag{3.10}$$

$\Delta_n f$ is the frequency variation of the light source. Replace $\Delta I_n$ in eq. (2.8) with eq. (3.11), and the error $\Delta\varphi$ is obtained:

$$\Delta\varphi = \sum_n \Delta_n f\times(\varphi+\phi_n)V\frac{w_n}{2}\left[1-\cos(2\varphi+2\phi_n)\right]. \tag{3.11}$$

Comparing with eqs. (3.5), (3.7), (3.9), (3.11), it is clear that the error distributions vary with the different error sources. To verify these mathematical solutions, the various error distributions are simulated in the next section.

## 4 Simulation verification and diagnosing method

The tested wavefront map for the simulation is shown in figure 1. The wavefront $\varphi$ is shown on the left and the tilt is removed. The intensity patterns are shown on the right. The Zernike coefficients of the wavefront are listed in table 1. The errors, including phase-shift error, position deviation caused by vibration, unstable intensity of the light source, and frequency fluctuation of the light source, are injected respectively into the intensity patterns. Peter de Groot proposed a thirteen-step algorithm (the phase-shifting step $\Delta\phi_n = \pi/2$) [14] with better robustness:

$$\varphi = \tan^{-1}\left(\frac{-3\,(I_1-I_{13})-4\,(I_2-I_{12})+12\,(I_4-I_{10})+21\,(I_5-I_9)+16\,(I_6-I_8)}{-4(I_2+I_{12})-12\,(I_3+I_{11})-12\,(I_4+I_{10})+16\,(I_6+I_8)+24I_7}\right). \tag{4.1}$$

Using this thirteen-step algorithm, the wavefront is extracted from the erroneous intensity patterns. The error $\Delta\varphi$ between the extracted wavefront and the real wavefront $\varphi$ is calculated (figure 2). The error distributions $\Delta\varphi$ caused by different error sources are separately illustrated in figure 2.

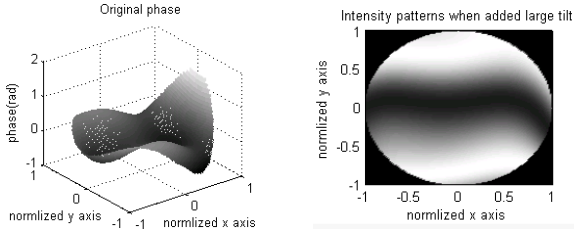


**Figure 1**. Wavefront map (tilt removed) and intensity patterns with tilt corresponding to the Zernike coefficients listed in table 1. There are two fringes in the intensity patterns.



2016 JINST 11 P05018

a) For the case of phase-shift error caused by the detuning error of the piezoelectric transducer or introduced by the vibration along the ray axis (figure 2 (A)), periodic ripples with doubled-frequency appears in the error distribution, comparing with the intensity patterns shown in figure 1. This result corresponds to the term $1 - \cos(2\varphi + 2\phi_n)$ in eq. (3.5).

b) For the case of position deviation caused by vibration (figure 2 (B)), the doubled-frequency ripples appears, but the same peak line is skewed in the other direction due to the terms $1 - \cos(2\varphi + 2\phi_n)$ and $\mathrm{d}^2\varphi \big/ (\mathrm{d}x\mathrm{d}y)$ in eq. (3.7).

c) For the case of unstable intensity in the light source (figure 2 (C)), there are modulated doubled-frequency ripples, and different ripples have different amplitudes (some are smaller, and some are larger, in a sine signal). This result is related to the term $\sin(\varphi + \phi_n) + V/2 \sin(2\varphi + 2\phi_n)$ in eq. (3.9).

d) For the case of frequency fluctuation in the light source (figure 2 (D)), the doubled-frequency ripples are also present. The amplitude of these ripples is not regular because of the term $(\varphi + \phi_n)$ in eq. (3.11). The amplitude of the ripple will increase in the tilt direction.

**Table 1**. Zernike coefficients used for the construction of a tested wavefront with tilt. The unit is radians.

| Zernike coefficient | Amount (rad) |
|---|---|
| $Z_3$ y tilt | 4 |
| $Z_4$ defocus | 0.2 |
| $Z_6$ primary astigmatism | 0.1 |
| $Z_7$ primary coma | 0.2 |
| $Z_{10}$ trefoil | 0.5 |
| $Z_{12}$ secondary astigmatism | 0.5 |

The five-step algorithm is simulated in the same way and has a same error distribution. The difference between the two algorithms lies only in the amount of the error. Due to space limitations, the detailed results of the five-step algorithm are not presented in this paper.

So that, an *in situ* method for diagnosing the error sources in phase shifting interferometer is proposed. The detail is listed as below:

a) A perfect tested surface ($< \lambda/20$ RMS, $\lambda$ is the wavelength) is selected for measurement. Tilt is added, and there are 2–4 fringes on the intensity patterns.

b) A method of averaging[1] is utilized for reduce the errors in several repeated measurements. Then, the error distribution $\Delta\varphi$ is obtained from the average result subtracting one measurement result.

c) According to the characteristics shown in figure 2, the error distribution can be distinguished and the error sources can be diagnosed.

[1] http://www.dtic.mil/dtic/tr/fulltext/u2/a258990.pdf.



2016 JINST 11 P05018

d) When the phase-shift error is constant, this processing needs more steps. One present measurement result subtracts the previous measurement result which was obtained when the interferometer worked well. The diversity between these two measurement results will show the phase-shift error (figure 2 (A)).

The method can be applied to fast diagnose and distinguish the error sources as follows: phase-shift error, position deviation caused by vibration, intensity instability of the light source, and frequency fluctuation of the light source.

| Item | Error source | Error Distribution | $\Delta\varphi$ |
|---|---|---|---|
| A | Phase-shift error | 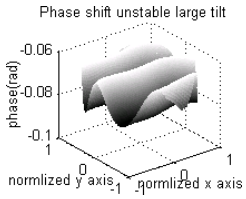  | $\Delta\varphi = \sum_n \Delta P_n \times V\frac{w_n}{2}[1-\cos(2\varphi+2\phi_n)]$ |
| B | Position deviation caused by vibration | 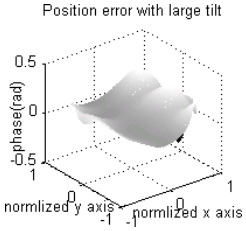  | $\Delta\varphi = \sum_n \frac{\mathrm{d}^2\varphi}{\mathrm{d}x\mathrm{d}y}\Delta x\Delta y V\frac{w_n}{2} \times [1-\cos(2\varphi+2\phi_n)]$ |
| C | Unstable intensity of the light source | 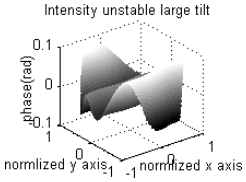  | $\Delta\varphi = \sum_n \Delta_n I(-w_n)\left[\sin(\varphi+\phi_n) + \frac{V}{2}\sin(2\varphi+2\phi_n)\right]$ |
| D | Frequency fluctuation of the light source | 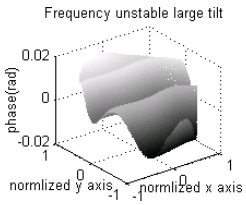  | $\Delta\varphi = \sum_n \Delta_n f(\varphi+\phi_n) \times V\frac{w_n}{2}[1-\cos(2\varphi+2\phi_n)]$ |

**Figure 2**. The 3D error distribution $\Delta\varphi$ caused by different error sources. (A) Phase-shift error, (B) Position deviation caused by vibration, (C) Unstable intensity of the light source, (D) Frequency fluctuation of the light source.

## 5 Verification testing

We impose vibration, phase-shift error, and intensity fluctuation into the comparison experiments by testing the same mirror with a ZYGO interferometer to verify this diagnosing method and those mathematical solutions.



2016 JINST 11 P05018

### 5.1 Position deviation caused by vibration

A plane with astigmatism (PV: 28.90 nm, RMS: 3.22 nm) was vertically placed on a stable platform. Different amounts of vibration were introduced into the experiments. The peak vibration velocity was 19.5 $\mu$m/s in the unstable situation, and 2 $\mu$m/s in the stable situation. To extract the errors from measurement, the average result over 32 measurements was taken as the real value. The error distribution $\Delta\varphi$ was obtained by subtracting one measurement from the average result. Figure 3 indicates the results of this experiment. Figure 3a shows the intensity patterns in the unstable situation; figure 3b shows the intensity patterns in the stable situation; figure 3c shows the error distribution $\Delta\varphi$ as the vibration velocity is 19.5 $\mu$m/s, and $\Delta\varphi$ is 0.02 $\lambda$ PV ($\lambda$=632.8 nm); figure 3c shows the intensity patterns in the stable situation; figure 3d is the wavefront error $\Delta\varphi$ caused by error sources in the stable situation, and $\Delta\varphi$ is 0.003 $\lambda$ PV; and figure 3e is the tested surface $\varphi$.

In figure 3c, there are 12 ripples in the error distribution, opposed to 6 fringes in the intensity figure 3a. These ripples are skewed in another direction. The quasi- astigmatism in figure 3b locates at 45° comparing the astigmatism at 0° in figure 3e. These features just coincide with the case of deviation caused by vibration (figure 2 (B)). Eq. (3.7) can explain the problem. The term $1-\cos(2\varphi+2\phi_n)$ introduced the doubled-frequency ripples. The term $\mathrm{d}^2\varphi\big/(\mathrm{d}x\mathrm{d}y)$, which is the derivative of $\varphi$, produces the quasi-astigmatism at 45°. The direction of vibration determines the rotation direction of $\mathrm{d}^2\varphi\big/(\mathrm{d}x\mathrm{d}y)$. When the vibration is depressed, that quasi-astigmatism vanishes in figure 3d. It is certain that the error caused by vibration disappears.

In figure 3d, there are 4 ripples opposed to 2 fringes on the intensity patterns. These ripples have different amplitudes, and fit the case of phase-shift error (figure 2 (C) and eq. (3.9)). But the amount of error is very little to take charge.

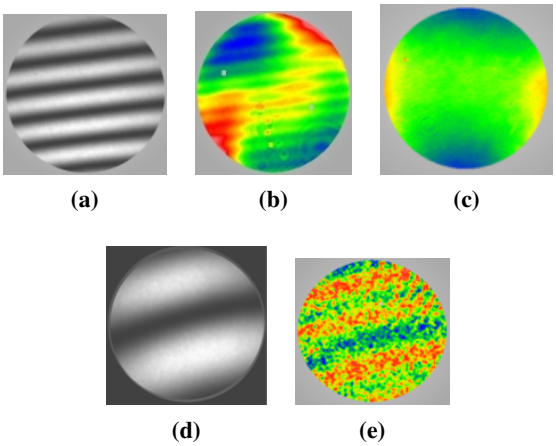


**Figure 3**. The intensity patterns and error distributions in different vibration situations. (a) Intensity patterns as the vibration velocity is 19.5 $\mu$m/s. (b) Intensity patterns as the vibration velocity is reduced to 2 $\mu$m/s. (c) The error distribution $\Delta\varphi$ as the vibration velocity is 19.5 $\mu$m/s. (d) The error distribution $\Delta\varphi$ as the vibration velocity is reduced to 2 $\mu$m/s. (e) The tested surface $\varphi$.

### 5.2 Phase-shift error

In the comparison experiment, we imposed phase-shift error into the interferogram. The error distribution was extracted and recorded following the method outlined in section 4. Figure 4



2016 JINST 11 P05018

displays the result of the comparison experiment. Figure 4a displays the intensity patterns with phase-shift error; figure 4b indicates the error distribution $\Delta\varphi$ with phase-shift error imposed, and the error amount is $0.02\lambda$; figure 4c shows the intensity patterns without phase-shift error. Figure 4d is the error distribution $\Delta\varphi$ without phase-shift error, and the error amount dropped to $0.005\lambda$.

In figure 4b, there are 4 periodic ripples in the error distribution, compared with 4 fringes in the intensity figure 4a. This fits the case of phase-shift error explained in section 4, corresponding to the term $1 - \cos(2\varphi + 2\phi_n)$ in eq. (3.5).

When the phase-shift error was removed, the periodic ripples disappeared in figure 3d with the contrast of the intensity patterns in figure 3c.

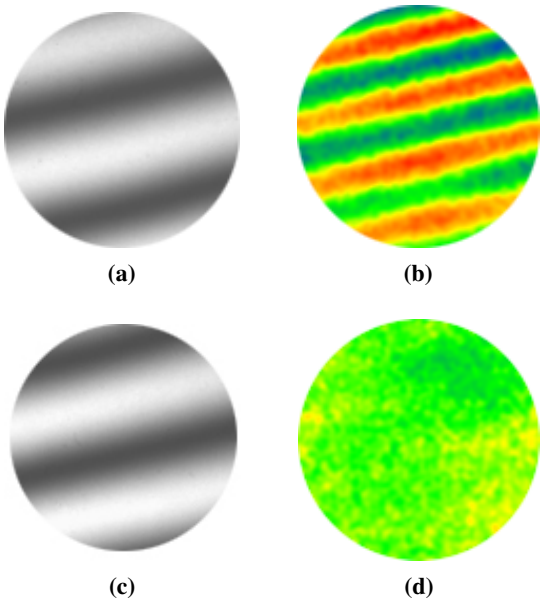


**Figure 4**. The intensity patterns and error distributions in the comparison experiment for the case of phase-shift error. (a) Intensity patterns with phase-shift error. (b) The error distribution $\Delta\varphi$ with phase-shift error. (c) Intensity patterns without phase-shift error. (d) The error distribution Intensity patterns without phase-shift error.

### 5.3 Unstable intensity

We imposed intensity fluctuation in the experiment. A silicon wafer wad tested with a GPI interferometer. The error distribution $\Delta\varphi$ ($0.01\lambda$) and the intensity patterns are shown in figure 5a and figure 5b respectively. Obviously, there are 8 ripples in figure 5a, comparing with 8 patterns in figure 5b.

The contrast $V$ of the intensity patterns is 0.2, eq. (3.9) is changed to: $\Delta\varphi = \sum_n \Delta_n I(-w_n) \cdot [\sin(\varphi + \phi_n) + 0.1\sin(2\varphi + 2\phi_n)]$, the term $0.1\sin(2\varphi + 2\phi_n)$ becomes very tiny. This will explain those 8 ripples in 2D error distribution.

## 6 Summary

To diagnose the error sources in phase shifting interferometry, the characteristics of errors must be analyzed. First, the variations of intensity patterns caused by different error sources are discussed.



2016 JINST 11 P05018

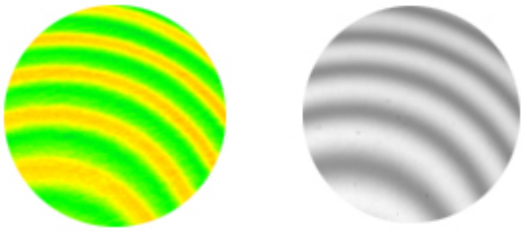

(a) (b)

**Figure 5**. The error distribution and intensity patterns for the case of unstable intensity. (a) 2D error distribution with the intensity fluctuation (b) the intensity patterns of the silicon wafer, the contrast $V$ of the interference fringes is about 0.2.

Phase extraction algorithm is based on the intensity patterns, and then the error distributions will vary. Next, the mathematical solutions of errors caused by different error sources were derived. The solutions show the diversity of error distributions. To demonstrate these solutions, the various error distributions caused by different error sources were simulated. The characteristics of the error distributions can be distinguished. An approach for diagnosing the error sources is proposed. In section 5, we impose vibration, intensity fluctuation and phase-shift error into the comparison experiments to demonstrate the validity of this approach. This *in situ* method can also be applied into an phase shifting interferometer with high precision, such as point diffraction interferometer [15, 16].

## Acknowledgments

We would like to acknowledge the financial support of the National Science and Technology Major Project.

## References

[1] Y. Du et al., *Circular common-path point diffraction interferometer*, *Optic. Lett.* **37** (2012) 3927.

[2] V.F. Paz et al., *Solving the inverse grating problem by white light interference Fourier scatterometry*, *Light Sci. Appl.* **1** (2012) e36.

[3] K. Otaki et al., *Accuracy evaluation of the point diffraction interferometer for extreme ultraviolet lithography aspheric mirror*, *J. Vac. Sci. Technol.* **B 20** (2002) 295.

[4] C.J. Evans, *Uncertainty evaluation for measurements of peak-to-valley surface form errors*, *CIRP Ann. Manuf. Tech.* **57** (2008) 509.

[5] J. Schwider et al., *Digital wave-front measuring interferometry: some systematic error sources*, *Appl. Opt.* **22** (1983) 3421.

[6] P. Hariharan, *Digital phase-stepping interferometry: effects of multiply reflected beams*, *Appl. Opt.* **26** (1987) 2506.

[7] J. van Wingerden, H.J. Frankena and C. Smorenburg, *Linear approximation for measurement errors in phase shifting interferometry*, *Appl. Opt.* **30** (1991) 2718.

[8] H. Schreiber and J.H. Bruning, *Phase Shifting Interferometry*, in *Optical Shop Testing*, D. Malacara ed., John Wiley & Sons, Inc. (2006), pp. 547–666.



2016 JINST 11 P05018

[9] K. Freischlad and C.L. Koliopoulos, *Fourier description of digital phase-measuring interferometry*, *J. Opt. Soc. Am.* **A 7** (1990) 542.

[10] D. Malacara, M. Servin and Z. Malacara, *Interferogram Analysis for Optical Testing*, 2nd edition, CRC Press, Taylor & Francis Group, Boca Raton U.S.A. (2005).

[11] C.P. Brophy, *Effect of intensity error correlation on the computed phase of phase-shifting interferometry*, *J. Opt. Soc. Am.* **A 7** (1990) 537.

[12] P.J. de Groot, *Vibration in phase-shifting interferometry*, *J. Opt. Soc. Am.* **A 12** (1995) 354.

[13] P.J. de Groot, *Derivation of algorithms for phase-shifting interferometry using the concept of a data-sampling window*, *Appl. Opt.* **34** (1995) 4723.

[14] P.J. de Groot, *Measurement of transparent plates with wavelength-tuned phase-shifting interferometry*, *Appl. Opt.* **39** (2000) 2658.

[15] J. Shao et al., *Study on evaluating the wavefront diffracted from an ultra small aperture*, *Optic. Precis. Eng.* **22** (2014) 2639 and online at http://www.eope.net/CN/abstract/abstract15478.shtml.

[16] J. Shao and D. Ma, *Testing the Criterion Wavefront Diffracted by Point Diffraction Interferometer*, *Chin. J. Laser.* **B 38** (2011) 0508003.

2016 JINST 11 P05018